



# Hyperon III: $K^- p - \pi \Sigma$ coupled-channel dynamics in the $\Lambda(1405)$ mass region

A. V. Anisovich<sup>1,2</sup>, A. V. Sarantsev<sup>1,2</sup>, V. A. Nikonov<sup>1,2</sup>, V. Burkert<sup>3</sup>, R. A. Schumacher<sup>4</sup>, U. Thoma<sup>1</sup>, E. Klempt<sup>1,a</sup>

<sup>1</sup> Helmholtz–Institut für Strahlen–und Kernphysik, Universität Bonn, 53115 Bonn, Germany

<sup>2</sup> National Research Centre “Kurchatov Institute”, Petersburg Nuclear Physics Institute, Gatchina 188300, Russia

<sup>3</sup> Thomas Jefferson National Accelerator Facility, Newport News, VA 23606, USA

<sup>4</sup> Carnegie Mellon University, Pittsburgh, PA 15213, USA

Received: 2 November 2019 / Accepted: 6 April 2020 / Published online: 19 May 2020

© The Author(s) 2020

Communicated by Nasser Kalantar-Nayestanaki

**Abstract** Low-energy data on the three charge states in  $\gamma p \rightarrow K^+(\Sigma\pi)$  from CLAS at JLab, on  $K^- p \rightarrow \pi^0\pi^0\Lambda$  and  $\pi^0\pi^0\Sigma$  from the Crystal Ball at BNL, bubble chamber data on  $K^- p \rightarrow \pi^-\pi^+\pi^\pm\Sigma^\mp$ , low-energy total cross sections on  $K^-$  induced reactions, and data on the  $K^- p$  atom are fitted with the BnGa partial-wave-analysis program. We find that the data can be fitted well with just one isoscalar spin-1/2 negative-parity pole, the  $\Lambda(1405)$ , and background contributions. In a fit with one isoscalar state, the  $\Lambda(1405)$  structure can be determined as a dominantly SU(3) singlet state. A fit with two isoscalar singlet states, with imposed properties of the low-mass state, is, however, also not incompatible with data.

## 1 Introduction

The  $\Lambda(1405)1/2^-$  resonance—here written as  $\Lambda(1405)$ —has been discussed controversially since its discovery in 1961 [1]: Dalitz et al. considered the  $\Lambda(1405)$  as a quasi-bound molecular state of the  $\bar{K}N$  system [2,3]. Tripp et al. [4] determined the relative signs of  $\bar{K}N \rightarrow \pi\Sigma$  transition amplitudes for  $\Sigma(1385)$ ,  $\Lambda(1405)$  and  $\Lambda(1520)$ , and identified  $\Lambda(1405)$  and  $\Lambda(1520)$  as mainly SU(3) singlet states. In quark models,  $\Lambda(1405)$  and  $\Lambda(1520)$  are interpreted as  $qqq$  resonances in which one of the quarks is excited to the  $p$  state forming a spin-doublet of states with a dominant SU(3)-singlet structure [5]. Later, Kaiser, Waas and Weise constructed an effective potential from a chiral Lagrangian, and the  $\Lambda(1405)$  emerged as quasi-bound state in the  $\bar{K}N$  and  $\pi\Sigma$  coupled-channel system [6]. Oller and Meissner [7] stud-

ied the  $S$ -wave  $\bar{K}N$  interactions in a relativistic chiral unitary approach based on a chiral Lagrangian. The Lagrangian was obtained from the interaction of the SU(3) octet of pseudoscalar mesons and the SU(3) octet of stable baryons. In their coupled-channel approach, they found two isoscalar resonances below 1450 MeV, at 1379.2 MeV as a mainly (96%) singlet state and at 1433.7 MeV as a mainly (76%) octet state, and one isovector resonance at 1444.0 MeV. The authors of Ref. [8] suggested that the two  $\Lambda^*$  poles as well as a third state at 1680 MeV are combinations of the singlet state and the two octet states expected in the  $8 \otimes 8$  into  $1 \oplus 8_s \oplus 8_a \oplus 10 \oplus \bar{10} \oplus 27$  decomposition. They interpreted the first wider state (at 1390 MeV in their analysis) as mainly singlet (53%), a second and a third state at 1426 MeV and 1680 MeV as mainly (69% and 78%, respectively) octet states. The isovector sector was found to be much more sensitive to the details of the coupled-channel approach [8]. Based on the approach used in [7], two poles were found at 1401 MeV and 1488 MeV [8], based on [9], one state was found at 1580 MeV. Here the other isovector state disappeared for dynamical reasons. The  $\Sigma$  resonances were interpreted as isovector companions of the isoscalar states. The findings presented in [7,8] were confirmed in a number of further studies. Here we quote a few recent papers [10–20]. A survey of the literature and a discussion of the different approaches can be found in Ref. [21].

In quark models [22–25], three isoscalar  $J^P = 1/2^-$  resonances are expected below 1.9 GeV.  $\Lambda(1405)$  is interpreted as the (mainly) SU(3) singlet state. The pole positions of the four-star  $\Lambda(1670) 1/2^-$  and of the three-star  $\Lambda(1800)1/2^-$  are found about 160 MeV above  $N(1535)1/2^-$  and  $N(1650)1/2^-$ , respectively. The former two states are commonly identified with the two expected (mainly) octet states [24]. The  $\Sigma(1620)1/2^-$  resonance is interpreted as

<sup>a</sup> e-mail: klempt@hiskp.uni-bonn.de (corresponding author)

the isospin partner of  $\Lambda(1670)1/2^-$  and  $\Sigma(1750)1/2^-$  as the isospin partner of  $\Lambda(1800)1/2^-$ . This interpretation is supported in a study of the spectrum of hyperon resonances [40,41]. The SU(3) symmetry of the quark model is thus experimentally confirmed. An assignment of the three resonances at 1380 MeV, 1426 MeV, and 1680 MeV to the quark model states with spin-parity  $1/2^-$ , instead of the  $\Lambda(1405)1/2^-$ ,  $\Lambda(1670)1/2^-$ , and  $\Lambda(1800)1/2^-$ , would be at variance with the quark model.

Several baryon resonances that can be generated dynamically like  $N(1440)1/2^+$ ,  $N(1535)1/2^-$ ,  $\Delta(1700)3/2^-$  are interpreted in [22–25] as quark-model states. With the identification of the negative-parity  $\Lambda$  resonances as outlined above, one of the two low-mass  $\Lambda$  states and the low-mass  $\Sigma$  state in [8,9] cannot be interpreted as quark-model states: the two states are supernumerous (and not required in the analysis presented here). Based on Regge phenomenology, the authors of Ref. [26] argue that the narrow state at about 1430 MeV fits into the common pattern of a linear Regge trajectory of known three-quark hyperons possibly indicating its three-quark nature. The wider state below  $\approx 1400$  MeV is speculated to be a pentaquark or of molecular nature.

The two-pole structure of the  $\Lambda(1405)$  region is not uncontested. All work before [7] assumed a single pole in this region. Later, HADES data on the reaction  $p + p \rightarrow \Sigma^+ + \pi^- + K^+ + p$  were successfully fitted with a single  $\Lambda(1405)$  at 1380 MeV [27]; it was shown that the peak cannot be assigned to  $\Sigma(1385)$ . This result was criticized in a subsequent reanalysis [28] where the mass was determined to  $1405_{-9}^{+11}$  MeV. The CLAS collaboration studied the three charge states in the reaction  $\gamma p \rightarrow K^+ \Sigma \pi$  [29] that provide precise information on the  $\Lambda(1405)$  line shape. Its spin and parity were determined in [30], until then taken from the quark model. The data were fitted in [29], the best fit was achieved with two low-mass isovector states ( $\Sigma^*$ 's) and one isoscalar state  $\Lambda(1405)$ . A reanalysis of these data showed that the data are also compatible with a standard single-pole  $\Lambda(1405)$  [31]. Dong, Sun and Pang [32] solved the Bethe–Salpeter equation in an unitary coupled-channel ansatz taking relativistic effects and off-shell corrections into account. In their model, the authors found that the off-shell corrections are very important. Without these, the authors reproduced the two-pole structure. Yet one pole disappeared when the off-shell corrections were switched on, and only one  $\Lambda(1405)$  survived. This contradicts [15,33]; in their ansatz, off-shell effects were found to be small and two poles were present. Revai [34,35] suggests that the two-pole structure is a consequence of the on-shell factorization approximation; without this approximation, only one pole was found. This conjecture was criticized very recently by Bruns and Cieplý [36]. Myint et al. [37] used a chiral model and found two poles in the  $\Lambda(1405)$  region. The peak structure in the data was assigned

to a single pole, while the second one provided a continuum background amplitude affecting the shape of the peak, but that pole was not interpreted as genuine resonance. We mention a study of the ratio of  $\Lambda(1405)$  and  $\Sigma(1385)$  in the photoproduction reactions  $\gamma p \rightarrow K^+ \Lambda \pi^0$  and  $K^+ \Sigma^\pm \pi^\mp$  [38].

Direct experimental evidence for the presence of two poles in the  $\Lambda(1405)$  region has been reported in Ref. [39]. The CLAS collaboration studied electroproduction of this resonance by studying the reaction  $e^- p \rightarrow e^- K^+(p\pi^0)\pi^-$  with the  $p\pi^0$  mass being compatible with  $\Sigma^+$  and with four-momentum transfers ranging from  $-t = 0.5$  to  $4.5$  GeV<sup>2</sup>. The data were shown for two subsets with  $1.0 < Q^2 < 1.5$  GeV<sup>2</sup> and  $1.5 < Q^2 < 3.0$  GeV<sup>2</sup>. The latter data were fitted with two incoherent Breit–Wigner functions with  $\Sigma\pi$  as only decay channel. The masses optimized at  $1.368 \pm 0.004$  GeV and  $1.423 \pm 0.002$  GeV (statistical fit errors only). A possible  $\Sigma(1385)3/2^+$  contribution was estimated to be small. The low- $t$  data set was not fitted simultaneously, and seem not describable with the same assumptions. Also the related chain  $e^- p \rightarrow e^- K^+(p\pi^-)\pi^0$ —which avoids possible  $\Sigma(1385)3/2^+$  contaminations—has not been investigated.

This work is part of a comprehensive study of the low-mass hyperon spectrum. In [40,41], we present a fit to existing data on  $K^- p$  induced reactions, evaluate the statistical evidence of contributing resonances, and report Breit–Wigner parameters and branching ratios as well as the properties of resonances at their poles. In [42], the resulting spectrum will be compared to quark model predictions. In [43], we shall explore the power of photoproduction to improve our knowledge on hyperons.

In this paper we present a partial wave analysis of data covering the  $\Lambda(1405)$  region. The data include the low-mass part of the  $\Sigma\pi$  system in the reaction  $\gamma p \rightarrow K^+ \Sigma \pi$  from JLab [29], data on the reaction  $K^- p \rightarrow \pi^0 \pi^0 \Sigma^0$  from BNL [44] and bubble chamber data on  $K^- p \rightarrow \pi^- \pi^+ \pi^\pm \Sigma^\mp$  [45], differential cross sections for  $K^- p \rightarrow K^- p$  and  $K^- p \rightarrow \bar{K}^0 n$  from [46], and the low-mass range for  $K^- p \rightarrow \pi \Sigma$  [47], total cross section measurements [48–51], ratios of  $K^- p$  capture rates [52,53], and the recent experimental results on the energy shift and width of kaonic hydrogen atoms constraining the  $K^- p$   $S$ -wave scattering length [54,55]. In spite of the large amount of data, data on  $K^- p$  interactions with a spin-polarized proton target are still missing. Hence the resulting scattering amplitudes remain model-dependent. Within the BnGa ansatz, the data are fully compatible with just one isoscalar resonance and conveniently chosen background amplitudes. A solution with two low-mass isoscalar poles describes the data with similar precision.

## 2 Formalism

In this section the basic features of the dispersion integration method are considered for the scattering amplitude. We start from the  $K$ -matrix method. This approximation extracts the leading singularities, it is a very popular approach in partial wave analyses. The pole and threshold singularities of the partial wave amplitude are taken into account, and the amplitude automatically satisfies unitarity. Here we describe the dynamical amplitude without the angular momentum tensors needed for non-vanishing angular momenta. The full amplitude is discussed in Matveev et al. [40]. We emphasize that the constraints from the symmetry-breaking pattern of low-energy QCD are not taken into account.

Although the  $K$ -matrix amplitude is an analytic function in the complex plane, it neglects left-hand singularities of the partial wave amplitude. Near thresholds, the  $K$ -matrix approach generates false kinematical singularities that need to be suppressed by imposing new assumptions. As a result, the  $K$ -matrix approach is not reliable in the low-energy region: this was clearly demonstrated in the analysis of the  $\pi\pi$   $S$ -wave scattering amplitude near the  $\pi\pi$  threshold [56,57].

### 2.1 Spectral integral equation for the $K$ -matrix amplitude

The  $K$ -matrix approach was introduced to satisfy directly the unitarity condition which is very important for an analysis of reactions near the unitarity limit. The  $S$ -matrix for the transition between the initial and the final state can be written as

$$S = (I + i\hat{\rho}\hat{K}) (I - i\hat{\rho}\hat{K})^{-1} = I + 2i\hat{\rho}\hat{K} (I - i\hat{\rho}\hat{K})^{-1}. \tag{1}$$

Here,  $\hat{\rho}$  is a diagonal matrix describing the phase volumes and  $\hat{K}$  is a real matrix that describes resonant and non-resonant contributions.

For the partial wave amplitude  $A(s)$  one obtains

$$\hat{A} = \hat{K} (I - i\hat{\rho}\hat{K})^{-1} = \hat{K} + \hat{K}i\hat{\rho}\hat{K} + \hat{K}i\hat{\rho}\hat{K}i\hat{\rho}\hat{K} + \dots \tag{2}$$

This equation can be also rewritten as

$$\hat{A} = \hat{A}i\hat{\rho}\hat{K} + \hat{K}. \tag{3}$$

The factor  $(I - i\hat{\rho}\hat{K})^{-1}$  describes the rescattering in the final state, it is inherent not only for scattering amplitudes but also for production amplitudes.

The elements of the  $K$ -matrix are parameterized as a sum of resonant terms (first-order poles) and non-resonant con-

tributions:

$$K_{ij} = \sum_{\alpha} \frac{g_i^{(\alpha)} g_j^{(\alpha)}}{M_{\alpha}^2 - s} + f_{ij}. \tag{4}$$

This form is defined by the symmetry condition and the condition that the scattering amplitude has pole singularities of the first order.

This approach allows us to distinguish between “bare” and “dressed” particles: due to rescattering, the bare particles, with poles on the real- $s$  axis, are transformed into particles dressed by a “coat” of mesons. In the  $K$ -matrix approach we deal with a “coat” formed by real particles. The contribution of virtual particles is included in the main part of the loop diagram,  $B(s)$ , discussed below, and is taken into account effectively by the renormalization of mass and couplings.

Let us discuss hadron–hadron scattering and the production amplitudes using the dispersion-relation (or spectral integral) technique. We write for the  $K$ -matrix amplitude a spectral integral equation that is an analog of the Bethe–Salpeter equation [59] for the Feynman technique. The spectral integral equation for the transition amplitude from the channel  $a$  to channel  $b$  is given by

$$A_{ab}(s) = \int \frac{ds'}{\pi} \frac{A_{aj}(s, s')}{s' - s - i\epsilon} \rho_j(s') K_{jb}(s', s) + K_{ab}(s). \tag{5}$$

Here,  $\rho_j(s')$  is a diagonal matrix of the phase volumes,  $A_{aj}(s, s')$  the off-shell amplitude and  $K_{jb}(s, s')$  the off-shell elementary interaction. The term  $-i\epsilon$  indicates that the integration is carried out in the complex plane just below the real axis.

The standard way of transforming Eq. (5) into a  $K$ -matrix form is the extraction of the imaginary and principal parts of the integral. The principal part has no singularities in the physical region and can be omitted (or taken into account by a renormalization of the  $K$ -matrix parameters):

$$\begin{aligned} & \int \frac{ds'}{\pi} \frac{A_{aj}(s, s')}{s' - s - i\epsilon} \rho_j(s') K_{jb}(s', s) \\ &= P \int \frac{ds'}{\pi} \frac{A_{aj}(s, s')}{s' - s} \rho_j(s') K_{jb}(s', s) \\ & \quad + iA_{aj}(s, s)\rho_j(s)K_{jb}(s) \rightarrow iA_{aj}(s, s)\rho_j(s)K_{jb}(s), \end{aligned} \tag{6}$$

where  $\int p$  is the principal-value integral. We thus obtain the standard  $K$ -matrix expression (3).

One of the easiest ways to take into account the real part of the integral in Eq. (6) (the so-called dispersion corrections) is to assume that the amplitude and the  $K$ -matrix have a trivial dependence on  $s'$ . Such a case corresponds, e.g., to a parameterization of the resonant couplings and non-resonant

$K$ -matrix terms by constants and to a regularization of the integral in Eq. (6) that depends on the scattering channel only by subtraction at a fixed energy. In this case we obtain

$$\int \frac{ds'}{\pi} \frac{A_{aj}(s, s')}{s' - s - i\epsilon} \rho_j(s') K_{jb}(s', s) = A_{aj}(s, s) \operatorname{Re} B(s) K_{jb}(s, s) + i A_{aj}(s, s) \rho_j(s) K_{jb}(s) \tag{7}$$

where

$$\operatorname{Re} B(s) = P \int^A \frac{ds'}{\pi} \frac{\rho_j(s')}{s' - s} \tag{8}$$

and  $A$  is a cutoff parameter. And for the transition amplitude we obtain

$$A = K (I - \operatorname{Re} B \hat{K} - i \hat{\rho} \hat{K})^{-1} S = (I - \operatorname{Re} B \hat{K} + i \hat{\rho} \hat{K}) (I - \operatorname{Re} B \hat{K} - i \hat{\rho} \hat{K})^{-1}. \tag{9}$$

This approach provides a correct continuation of the amplitude below thresholds. The  $B$ -matrix is calculated approximately using a  $D$  matrix.

### 2.2 The $D$ -matrix approach

As we discussed above, the  $K$ -matrix approach can be considered as an effective way to calculate an infinite sum of rescattering diagrams from the spectral integral equation. The rescattering diagrams can be divided into  $K$ -matrix blocks which describe a transition from one channel into another one. Thus the rank of the  $K$ -matrix is defined by the number of the channels taken into account explicitly. The key issue of the  $K$ -matrix approach is a factorization of vertices and loop diagrams. The factorization is automatically fulfilled for the imaginary part, and in many cases a contribution from the real part is neglected. When the vertices have a non-trivial energy dependence, the real part cannot be separated from the  $K$ -matrix block and another approach should be used to calculate the amplitude. The most straightforward idea is to extract blocks which describe a transition from one “bare” state to another one. Then factorization is automatically fulfilled for the pole terms.

Let us introduce the block  $D_{\alpha\beta}$  which describes a transition between the bare state  $\alpha$  (but without the propagator of this state) and the bare state  $\beta$  (with the propagator of this state included). For such a block one can write the following equation:

$$D_{\alpha\beta} = D_{\alpha\gamma} \sum_j B_{\gamma\delta}^j d_{\delta\beta} + d_{\alpha\beta} \tag{10}$$

Or, in the matrix form,  $\hat{D} = \hat{D} \hat{B} \hat{d} + \hat{d} = \hat{d} (I - \hat{B} \hat{d})^{-1}$  Here, the  $\hat{d}$  is a diagonal matrix of the propagators

$$\hat{d} = \operatorname{diag} \left( \frac{1}{M_1^2 - s}, \frac{1}{M_2^2 - s}, \dots, \frac{1}{M_N^2 - s} \right)$$

where  $N$  is the number of resonant terms. The elements of the  $\hat{B}$ -matrix are equal to

$$\hat{B}_{\alpha\beta} = \sum_j B_{\alpha\beta}^j = \sum_j \int_{(m_{1j}+m_{2j})^2}^{\infty} \frac{ds'}{\pi} \frac{g_j^{R(\alpha)} \rho_j(s', m_{1j}, m_{2j}) g_j^{L(\beta)}}{s' - s - i0}. \tag{11}$$

The  $g_j^{R(\alpha)}$  and  $g_j^{L(\alpha)}$  are right and left vertices for a transition from the bare state  $\alpha$  to the channel  $j$ . The function  $B_{ab}^j$  depends on initial, intermediate and final states and allows us to introduce for every transition a specific energy dependence and regularization procedure.

For the resonance transition the right and left vertices are the same:

$$g_j^{R(\alpha)} = g_j^{L(\alpha)} = g_j^{(\alpha)} \tag{12}$$

The scattering amplitude between channels  $i$  and  $j$  which are taken into account in the rescattering has the form

$$A_{ij} = g_i^{(\alpha)} \hat{D}_{\beta\gamma} g_j^{(\gamma)}. \tag{13}$$

In the case of a single resonance we obtain the equation

$$A_{ij} = \frac{g_i^{(1)} g_j^{(1)}}{M^2 - s} \left( 1 - \frac{\sum_k B_{11}^k}{M^2 - s} \right)^{-1} = \frac{g_i^{(1)} g_j^{(1)}}{M^2 - s - \sum_k B_{11}^k}. \tag{14}$$

The elements of the  $B_{\alpha\beta}^j$  can be calculated using a subtraction procedure:

$$B_{\alpha\beta}^j(s) = B_{\alpha\beta}^j(M_j^2) + (s - M_j^2) \times \int_{(m_j+m_{Bj})^2}^{\infty} ds' \frac{g_j^{(\alpha)} \rho_j(s', m_j, m_{Bj}) C_j(s', m_j, m_{Bj}) g_j^{(\beta)}}{\pi (s' - s - i\epsilon)(s' - M_j^2)}. \tag{15}$$

Here, the subtraction constants  $B_{\alpha\beta}^j(M_j^2)$  are set to zero.

For an  $S$ -wave amplitude, the terms  $\rho_j(s', m_j, m_{Bj})$  and  $C_j(s', m_j, m_{Bj})$  are equal to

$$\rho(s) = \frac{2|\mathbf{k}| m_{Bj} + k_{0Bj}}{\sqrt{s} 2m_{Bj}},$$

$$C_j(s', m_j, m_{Bj}) = \sqrt{\frac{1.5}{1 + |\mathbf{k}|^2}}, \tag{16}$$

where  $|\mathbf{k}|$  is the relative momentum and  $k_{0Bj}$  is the baryon energy in the center-of-mass system.

In the fit to the  $K^-p$  elastic and charge-exchange cross sections, amplitudes for  $P$ -wave partial waves with isospin quantum numbers zero and one are included. These waves are found to be small; they are considered to be a background here. The  $P$ -wave contributions are included in the form of a Breit–Wigner amplitude with a subthreshold mass. The  $D$ -wave is represented by one relativistic Breit–Wigner amplitude at about 1520 MeV.

### 2.3 Fit to photoproduction data

The leading singularity in reactions with a resonance in a three-body final state is given by the resonance pole. The next leading singularity is a triangle singularity which develops when one particle from the resonance decay interacts with the third particle. The full process can be described by a  $P$ -vector amplitude. In the  $K$ -matrix approach it has the form

$$A_a = \hat{P}_b (\hat{I} - i\hat{\rho}\hat{K})_{ba}^{-1}. \tag{17}$$

The vector  $\hat{P}$  is parameterized in the form

$$P_b = \sum_{\alpha} \frac{G^{(\alpha)} g_b^{(\alpha)}}{M_{\alpha}^2 - s} \tag{18}$$

where  $M_{\alpha}, g_a^{(\alpha)}$  are the mass and decay couplings of the resonance  $\alpha$  into two-particle final state. The production of the resonance is described by the couplings  $G^{(\alpha)}$  which could be functions of energy. In the case of a narrow resonance, the  $G^{(\alpha)}$  can be approximated by a constant; we choose it as a complex number. Its phase describes effectively contributions from complicated processes such as triangle singularities. In photoproduction reactions, the  $G^{(\alpha)}$  depend on the partial wave which is produced in the  $\gamma p$  channel.

Here, the reaction  $\gamma p \rightarrow K^+(\Sigma\pi)$  is considered. The photon energy is high and a wide range is covered. The dynamics of the initial state is unknown. Hence all partial waves up to  $J^P = 7/2^{\pm}$  are taken into account. For the  $\gamma p$  system in  $J = 1/2$ , one helicity amplitude contributes, while for  $J > 1/2$ , two helicity amplitudes contribute. In each of the eight partial waves, we allow for two Breit–Wigner amplitudes with free masses and widths and complex couplings to the isobars. However, we describe not only the  $\Lambda(1405)$  region but fit the full mass range of the  $\Sigma\pi$  system,

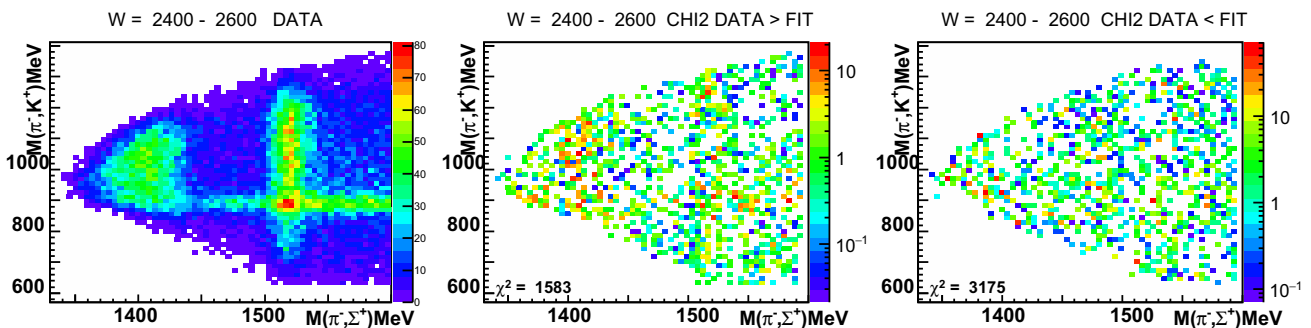


**Fig. 1**  $\gamma p \rightarrow K^+\pi^-\Sigma^+$  for  $2400 < W = M_{\gamma p} < 2600$  MeV:  $M(\pi^-K^+)$  versus  $M(\pi^-\Sigma^+)$  two-dimensional mass distributions, left: reconstructed data without acceptance correction, middle:  $\chi^2$ -

distributions for the case where the data exceed the fit and (right) where the fit exceeds the data. The total  $\chi^2$  is given in the left corner of the subfigures. The number of cells with entries is 2001

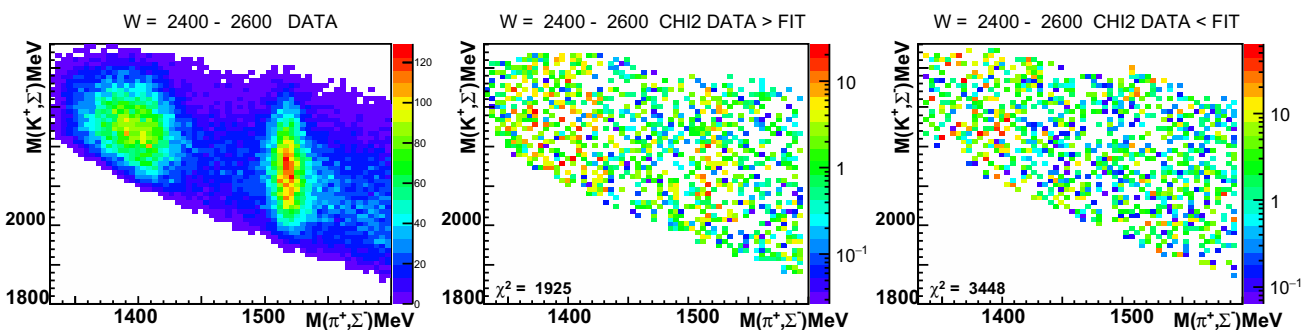


**Fig. 2**  $\gamma p \rightarrow K^+\pi^+\Sigma^-$  for  $2400 < W = M_{\gamma p} < 2600$  MeV:  $M(K^+\Sigma^-)$  versus  $M(\pi^+\Sigma^-)$  two-dimensional mass distributions, left: reconstructed data without acceptance correction, middle:  $\chi^2$ -

distributions for the case where the data exceed the fit and (right) where the fit exceeds the data. The total  $\chi^2$  is given in the left corner of the subfigures. The number of cells with entries is 1963

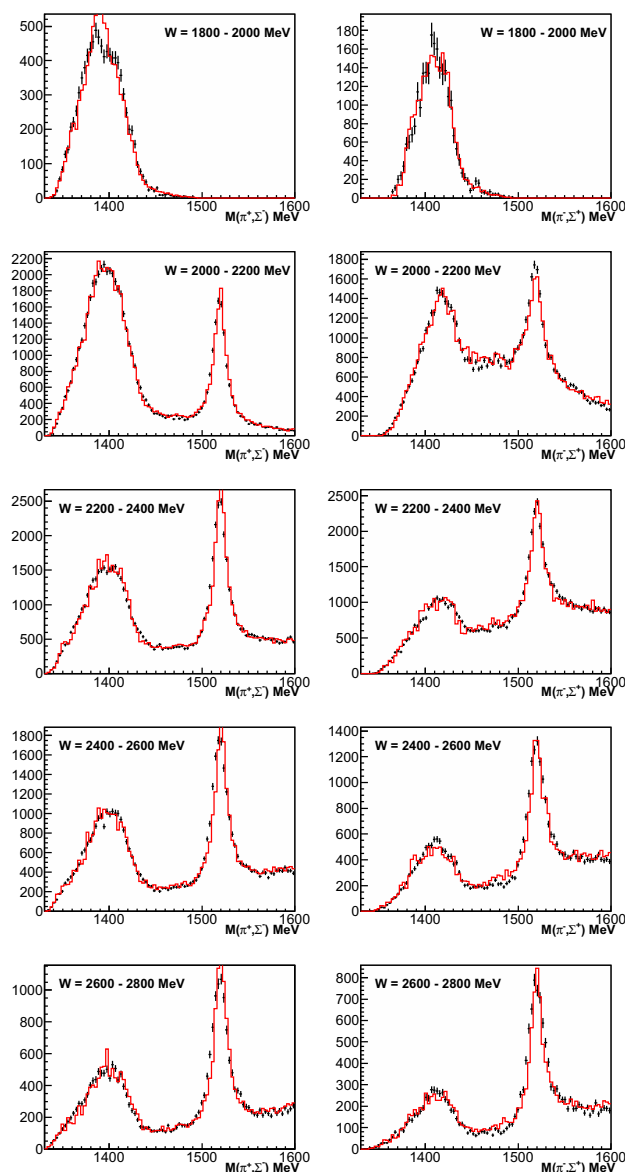


**Fig. 3** The  $\pi^+\Sigma^-$  (left),  $\pi^-\Sigma^+$  (right) invariant mass distributions from the reaction  $\gamma p \rightarrow K^+\Sigma\pi$  [29], given as number of events per 3 MeV. The data are fitted in a likelihood fit to individual events. The fit, represented by the histograms (red), uses one pole to describe  $\Lambda(1405)$

hence the helicity amplitudes and the Breit–Wigner mass and width are determined from a larger data set than discussed here.

#### 2.4 $\Lambda(\frac{1}{2}^-)$ and $\Sigma(\frac{1}{2}^-)$ partial waves parameterizations

We are interested in the amplitude behavior in the region from the  $\pi\Sigma$  threshold to  $\sqrt{s} \sim 1.5$  GeV. Hence both  $I = 0$  and  $I = 1$  amplitudes could contain one or two poles. The fit should tell us where the poles of the amplitudes are located. The  $\Lambda(\frac{1}{2}^-)$  amplitude is described by a five-channel

amplitude with possible decays to  $\pi^-\Sigma^+$ ,  $\pi^0\Sigma^0$ ,  $\pi^+\Sigma^-$ ,  $K^-p$  and  $K^0n$ . The constructed amplitudes take into account isotopic mass differences (threshold positions) but neglect Coulomb interactions. From pion scattering off protons we know that Coulomb interference with the hadronic amplitude is important only in the very forward region, a region for which, at present, no data exist.

### 3 Fits to the data

The mass of  $\Lambda(1405)$  falls below the  $K^-p$  threshold. In  $K^-p$  induced reactions only the high-mass part of  $\Lambda(1405)$  can be produced. An important role for the study of  $\Lambda(1405)$  is hence provided by the CLAS results on  $\gamma p \rightarrow K^+\Sigma^+\pi^-$ ,  $K^+\Sigma^0\pi^0$ , and  $K^+\Sigma^-\pi^+$  [29] where the full  $\Lambda(1405)$  shape can be studied. Figures 1 (left) and 2 (left) show selected two-dimensional mass distributions:  $M_{\pi^-K^+}$  versus  $M_{\pi^-\Sigma^+}$  and  $M_{K^+\Sigma^-}$  versus  $M_{\pi^+\Sigma^-}$  for a  $\gamma p$  invariant mass in the 2400–2600 MeV range. In both figures, a vertical band is seen at  $M_{\Sigma^+\pi^-}$  or  $M_{\Sigma^-\pi^+} \approx 1.52$  GeV: the  $\Lambda(1520)$ . At low masses, a broad enhancement due to  $\Sigma(1385)$  and  $\Lambda(1405)$  is seen which both decay into  $\Sigma^\pm\pi^\mp$ . A horizontal band in Fig. 1 is evidence that we have  $K^*$  production. The  $K^*$  band interferes with  $\Sigma(1385)$ ,  $\Lambda(1405)$ , and  $\Lambda(1520)$ . The resonances  $K^*$ ,  $\Sigma(1385)$  and  $\Lambda(1520)$  are described by relativistic Breit–Wigner amplitudes.

In Fig. 2 (left), the  $M_{K^+\Sigma^-}$  invariant mass is plotted against  $M_{\Sigma^-\pi^+}$ . There are no longer striking horizontal bands which would indicate  $\Sigma^-K^+$  resonances. There is also no  $K^+\pi^+$  band that would show up as a band in the counterdiagonal.

The data were fitted event by event in a likelihood fit. The center and right subfigures in Figs. 1 and 2 show the  $\chi^2$  per bin for events in which the data exceed the fit and for events in which the fit exceeds the data. The total  $\chi^2$  of the fit to the full data set covering the  $W$  range from 1800 to 2800 MeV is moderate: it is 41,320 for 16,076 cells. However, no significant pattern is seen in the difference plots. Hence we believe the fit to be acceptable.

Figure 3 shows the two  $\Sigma^\pm\pi^\mp$  mass distributions and the BnGa fit. The  $\Lambda(1520)$  resonance is clearly seen. The low-mass structure contains contributions from  $\Lambda(1405)$  and from  $\Sigma(1385)$ . The result of the fit was then used to predict the  $\Sigma^0\pi^0$  mass distribution for events from  $\gamma p \rightarrow K^+\Sigma^0\pi^0$ . Data and prediction are shown in Fig. 4. The fit identifies the two components reliably; the prediction for the  $\pi^0\Sigma^0$  mass distribution is very good: this distribution contains no  $\Sigma(1385)$  since the decay  $\Sigma(1385) \rightarrow \pi^0\Sigma^0$  is forbidden.

Before the CLAS data became available, the full  $\Lambda(1405)$  mass distribution was accessible from old bubble chamber data on  $K^-p \rightarrow \pi^-\pi^+\pi^\pm\Sigma^\mp$  [45]. The  $\Lambda(1405)$  was

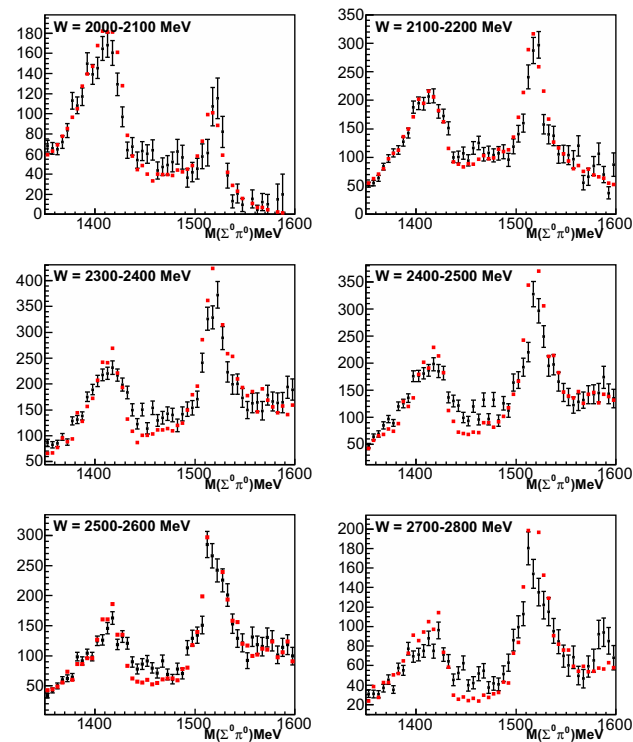


**Fig. 4** The  $\pi^0 \Sigma^0$  mass distribution [29] is given as weighted number of events per 5 MeV. The data are not included in the fit, the prediction is represented by (red) dots

observed in the  $K^- p \rightarrow \pi^- \Sigma^+(1670)3/2^-, \Sigma^+(1670)3/2^- \rightarrow \pi^+ \Lambda(1405)$  cascade, with  $\Lambda(1405)1/2^- \rightarrow \pi^\pm \Sigma^\mp$ . In the fit, a  $\approx 25\%$  fraction of  $\Sigma^0(1385)$  was admitted. The data are well reproduced by our fit with  $\chi^2/(N_{\text{data}} - N_{\text{param.}}) = 3.3/(12 - 7)$  (see Fig. 5).

The Crystal Ball collaboration at BNL studied the reactions  $K^- p \rightarrow \pi^0 \pi^0 \Lambda$  and  $K^- p \rightarrow \pi^0 \pi^0 \Sigma^0$  [44]. The events were fitted maximizing the likelihood in an event-by-event fit. The fit assumed that the reactions proceed via formation of  $\Lambda(1600)1/2^+, \Lambda(1670)1/2^-$  and  $\Lambda(1690)3/2^-$  or via  $\Sigma(1660)1/2^+$  and  $\Sigma(1670)3/2^-$ . These resonances have several decay chains leading to the final states studied at BNL (see, e.g., [40,41]).

Figure 6 shows the  $\pi^0 \Lambda$  and  $\pi^0 \Sigma^0$  invariant mass distributions and the fit. In the  $\pi^0 \Lambda$  distribution, the  $\Sigma(1385)$  dominates the reaction, a peak in the  $\pi^0 \Sigma^0$  mass distribution provides evidence for  $\Lambda(1405)$ . The data are well reproduced by the fit. The BNL data had been fit by the authors of Magas et al. [60]. The fit describes qualitatively the  $\pi^0 \Sigma^0$  mass projection and the total cross section. The authors conclude that the data are compatible with two poles in the  $\Lambda(1405)$  region.

$K^- p$  scattering starts at 1432 MeV, above the nominal mass of  $\Lambda(1405)$ . Nevertheless, kaon-induced reactions provide significant constraints on the  $I(J^P) = 0(1/2^-)$ -

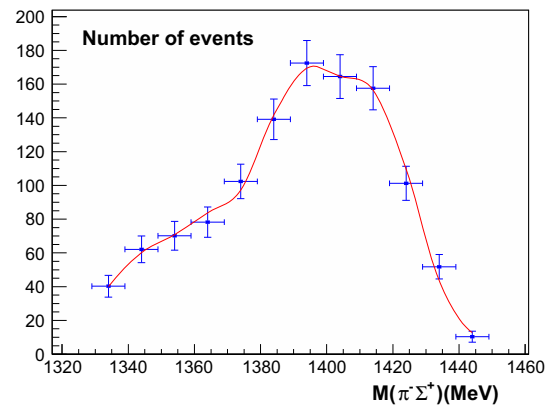


**Fig. 5**  $\Sigma^+ \pi^-$  mass projection from the reaction  $K^- p \rightarrow \pi^- \pi^+ \pi^\mp \Sigma^\pm$  for events with  $M_{\pi^+ \pi^\pm}$  compatible with  $\Sigma(1670)3/2^-$  [45]. Shown is the number of events per 10 MeV

amplitude. Figure 7 shows the differential cross section for  $K^- p \rightarrow K^- p$  and  $K^- p \rightarrow \bar{K}^0 n$  from [46] in selected bins of the invariant mass. The data are reasonably well described even though the fit underestimates the low-energy elastic cross section. This is enforced by the strong-interaction width of the  $K^- p$  atom (see below) which we insist in the fit to be described by the global fit. At 1524 MeV, the angular distribution reveals the dominance of  $\Lambda(1520)$  in this mass region. The underestimation of the total cross section could be due to an additional resonance that we might miss in our analysis. Fits based on Effective Field Theories describe these data with better precision. We imposed a second low-mass isoscalar resonance with mass and width compatible with the results from Refs. [12,13]. The fit to the elastic scattering data improved significantly, the CLAS data were described with less accuracy (see Sect. 4.2).

Figure 7 also shows the differential cross section for  $K^- p \rightarrow \pi^+ \Sigma^-, K^- p \rightarrow \pi^0 \Sigma^0$ , and  $K^- p \rightarrow \pi^- \Sigma^+$  in the low-energy region [47]. Data on these reactions covering the full  $\Lambda(1520)$  range do not exist but the influence of this resonance is clearly seen in the lowest-mass bin covering the 1532 to 1540 MeV mass range. This data is decisive for the interpretation of the  $\Lambda(1405)$  as (mainly) SU(3) singlet or octet state.

Figure 8 shows the total cross sections for  $K^- p$  induced reactions:  $K^- p \rightarrow K^- p, K^- p \rightarrow \bar{K}^0 n, K^- p \rightarrow \pi^0 \Lambda, K^- p \rightarrow \pi^+ \Sigma^-, K^- p \rightarrow \pi^0 \Sigma^0, K^- p \rightarrow \pi^- \Sigma^+$  [48–51]. The data are restricted to the low-mass region, with  $K^-$  laboratory momentum  $P_{\text{lab}} < 300$  MeV, where the  $P$ -wave scattering amplitude can be neglected. Note that the fit curve for the elastic scattering total cross section is rather determined by the differential cross section of the data from [46] and hardly influenced by the data on the total cross section.

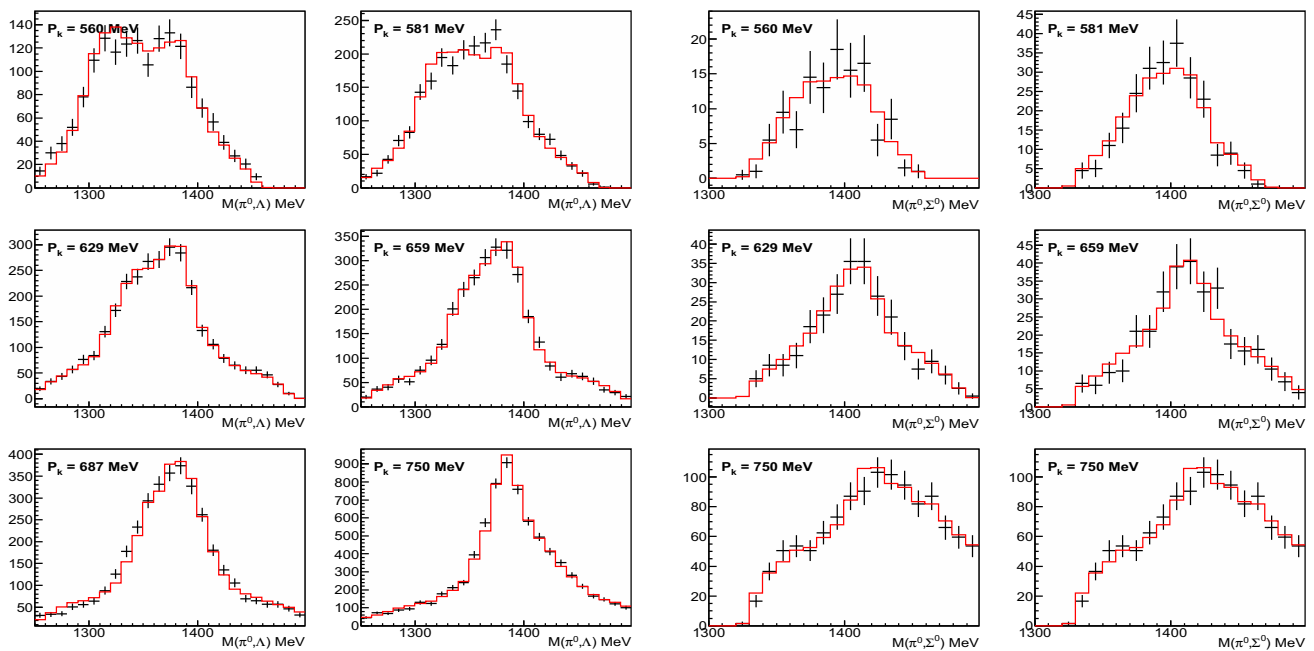


**Fig. 6** The Crystal Ball data on  $K^- p \rightarrow \pi^0 \pi^0 \Lambda$  (left) and  $K^- p \rightarrow \pi^0 \pi^0 \Sigma^0$  (right) [44] shown as black data points. One pole solution is presented as histogram (red)

The fits are constrained by properties of the  $K^- p$  system at rest. The SIDDHARTA experiment at DAΦNE determined the energy shift and width of the 1S level of the kaonic hydrogen atom [54, 55]. The values (Eq. (20a)) are related to the  $K^- p$  scattering length via the modified Deser-type formula [61]:

$$\Delta E - i\Gamma/2 = -2\alpha^3 \mu_c^2 a_{K^- p} [1 - 2a_{K^- p} \alpha \mu_c (\ln \alpha - 1)], \tag{19}$$

where  $\alpha \simeq 1/137$  is the fine-structure constant,  $\mu_c$  is the reduced mass and  $a_{K^- p}$  the scattering length of the  $K^- p$  system. From Refs. [52, 53], we take decay ratios listed in Eqs. (20b)–(20d). The quantities listed in Eqs. (20) are compared to the fit in Table 1. We have

$$\Delta E - i\Gamma/2 = (283 \pm 42) - i(271 \pm 55) \text{ eV} \tag{20a}$$

$$\gamma = \frac{\Gamma_{K^- p \rightarrow \pi^+ \Sigma^-}}{\Gamma_{K^- p \rightarrow \pi^- \Sigma^+}} = 2.38 \pm 0.04, \tag{20b}$$

$$R_n = \frac{\Gamma_{K^- p \rightarrow \pi^0 \Lambda}}{\Gamma_{K^- p \rightarrow \text{neutral}}} = 0.189 \pm 0.015 \tag{20c}$$

$$R_c = \frac{\Gamma_{K^- p \rightarrow \pi^\pm \Sigma^\pm}}{\Gamma_{K^- p \rightarrow \text{inelastic}}} = 0.664 \pm 0.011. \tag{20d}$$

Below we discuss two solutions with different pole structures. In our one-pole solution the isoscalar amplitude is described by a one-pole D-matrix amplitude that depends on two real coupling constants ( $g_{\pi \Sigma}$  and  $g_{KN}$ ) and a bare mass value  $M$ . In our two-pole solution, we have D-matrix ampli-

tude with two poles. The  $\Sigma(\frac{1}{2}^-)$  amplitude has two poles and three decay channels, so we have a three-channel amplitude that depends on eight fit parameters. For  $K^- p$  scattering, we allow for a small  $P$ -wave contribution. The  $P$ -wave is described by one isoscalar and one isovector subthreshold pole, both with two coupling constants.

The production mechanism of the reaction  $\gamma p \rightarrow K^+ \Sigma \pi$  is not known. We describe the initial state by two Breit-Wigner amplitudes in each partial wave for  $J^P = 1/2^\pm, 3/2^\pm, 5/2^\pm,$  and  $7/2^\pm$  and free coupling constants for their decays into  $\Sigma(1385)\bar{K}, \Lambda(1405)\bar{K}, \Lambda(1520)\bar{K},$  or  $\Sigma K^*$ . Thus the photoproduction dynamics is governed by a very large number of parameters. The properties of  $\Sigma(1385)$  and  $K^*$  are taken from the RPP [58].

The reactions studied at BNL are much lower in mass. The only required intermediate states are  $\Sigma(1385)3/2^+ \pi^0, \Lambda(1405)\pi^0, \Lambda(1520)\pi^0, \Sigma(\pi\pi)_{S\text{-wave}},$  and  $\Lambda(\pi\pi)_{S\text{-wave}}$  involving 24 additional parameters.

The CLAS data on three-body final states are, of course, more complicated to analyze; effects like three-body unitarity are not considered in this analysis. Surprisingly, the results hardly changed when these data were excluded. The bubble chamber data from [45] had practically no impact on the fit; the data were included for historical reasons.

For the  $\Sigma(\frac{1}{2}^-)$  partial wave, we use a two-pole parameterization. Both poles move far away from the physical region and describe background processes, likely due to  $t$  and/or  $u$ -channel exchange processes. We do not need poles in the



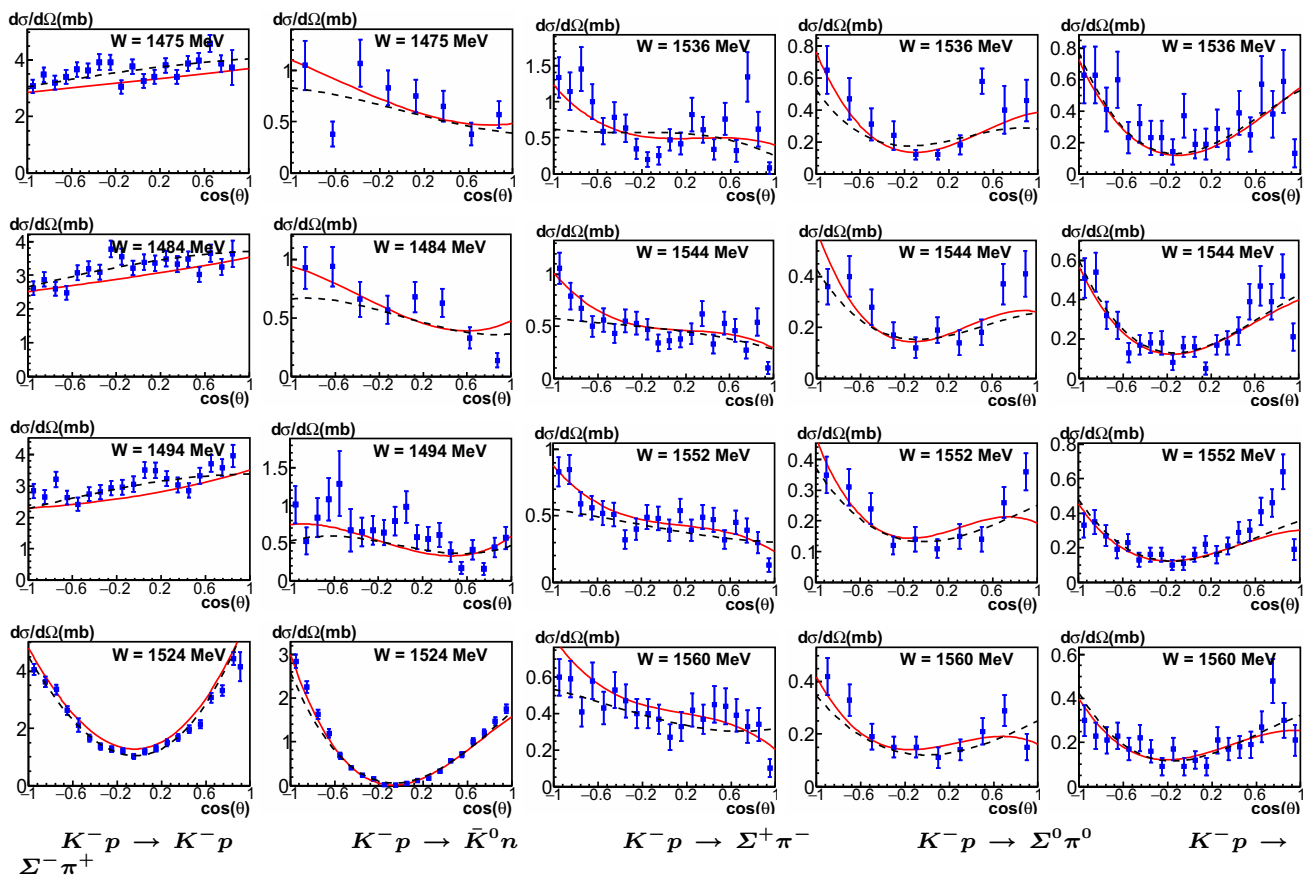


**Fig. 7** Selected differential cross sections for (from left to right)  $K^-p \rightarrow K^-p$ ,  $K^-p \rightarrow \bar{K}^0n$ ,  $\Sigma^+\pi^-$ ,  $\Sigma^0\pi^0$ , and  $\Sigma^-\pi^+$ . The data on  $K^-p \rightarrow \bar{K}N$  were taken between 1464 and 1548 MeV invariant mass and reported in 25 bins from [46]. Fitted was the full range, shown here

are three bins. The data on  $\Sigma\pi$  covering the 1532 to 1700 MeV mass range were reported in Ref. [47]. For this reaction, only the data shown are included in the fit. The one-pole fit is given by the solid, the two-pole fit by the dashed curve

$\Sigma(\frac{1}{2}^-)$  amplitude in the region from the  $\pi\Sigma$  threshold to 1500 MeV.

### 4 Results for the isoscalar amplitude

To find the pole positions in the  $\Lambda(\frac{1}{2}^-)$  wave in the region below 1500 MeV, we performed one-pole and two-pole fits. In all solutions, we find one leading pole position of the  $\Lambda(1405)$ . Its position is rather stable. The pole of the  $\Lambda(1520)3/2^-$  is hardly affected when the number of poles in the  $J^P = 1/2^-$  wave is changed.

#### 4.1 One-pole solution

The one-pole fit describes the data convincingly. The pole properties  $\Lambda(1405)$  and  $\Lambda(1520)$  are collected in Table 2. The transition residues for the transition from the initial are defined as

$$\text{Res}(\bar{K}N \rightarrow \Lambda^* \rightarrow \text{final}) = \frac{g_i g_f}{2W_{\text{pole}}} \sqrt{\rho_i \rho_f} \quad (21)$$

where  $W_{\text{pole}}$  represents the pole mass and  $\rho_i, \rho_f$  are the initial- and final-state phase spaces. The small phases are due to the position of the pole in the complex plane. The four  $D$ -matrix coupling constants are real and positive.

Finally, we performed a fit in which the product sign of the  $D$ -matrix element for  $\bar{K}N \rightarrow \Lambda(1405) \rightarrow \pi\Sigma$  was forced to stay negative. The  $\chi^2$  of the fit for the data on  $K^-p \rightarrow \pi\Sigma$  deteriorated from  $\chi^2 = 313$  to  $\chi^2 = 563$  for 200 data points. We find the latter fit to be unacceptable. In our one-pole solution,  $\Lambda(1405)$  has an SU(3) structure that is dominated by its singlet component.

#### 4.2 Two-pole solution

The two-poles hypothesis fit gives a slightly better description but we did not find a solution with two pole positions in the 1300–1450 MeV region. When a second pole was

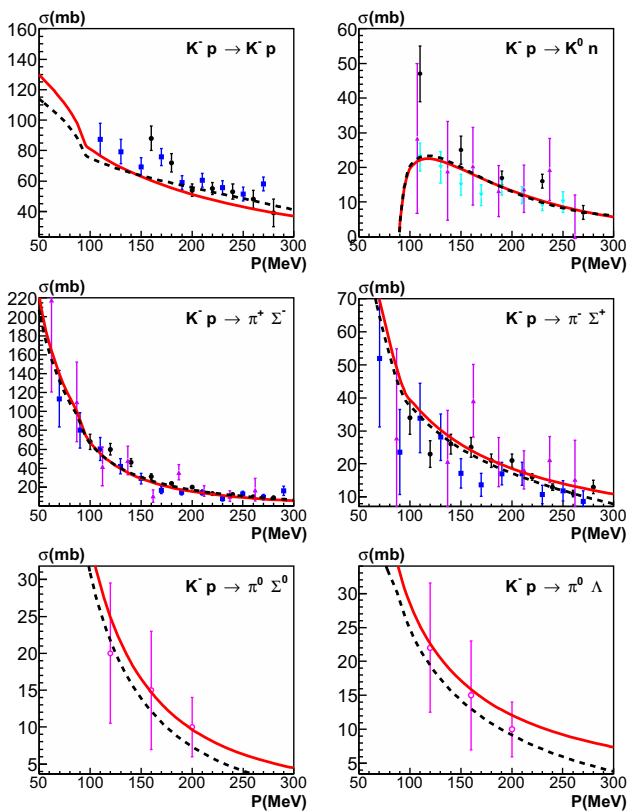


**Fig. 8** The total cross sections for  $K^-p$  induced reactions:  $K^-p \rightarrow K^-p$ ,  $K^-p \rightarrow \bar{K}^0n$ ,  $K^-p \rightarrow \pi^0\Lambda$ ,  $K^-p \rightarrow \pi^+\Sigma^-$ ,  $K^-p \rightarrow \pi^+\Sigma^+$ ,  $K^-p \rightarrow \pi^0\Sigma^0$ ,  $K^-p \rightarrow \pi^-\Sigma^+$  [48–51]. The single-pole  $\Lambda(1405)$  fit is given as the red curve

**Table 1** Experimental results for the quantities listed in Eq. (20) and the fit result

	Data	Fit
$\Delta E - i\Gamma/2$	$283 \pm 42 - i(271 \pm 55) \text{ eV}$	$308 \pm 15 - i(336 \pm 15) \text{ eV}$
	Two-pole solution	$292 \pm 15 - i(312 \pm 15) \text{ eV}$
$\gamma$	$2.38 \pm 0.04$	$2.40 \pm 0.02$
	Two-pole solution	$2.37 \pm 0.02$
$R_n$	$0.189 \pm 0.015$	$0.209 \pm 0.008$
	Two-pole solution	$0.200 \pm 0.008$
$R_c$	$0.664 \pm 0.011$	$0.668 \pm 0.010$
	Two-pole solution	$0.674 \pm 0.010$

admitted in the fit, it moved into the non-physical region below the  $\pi\Sigma$  threshold, and the pole can be considered as a non-resonant background contribution; alternatively, the pole moved to the  $K^-p$  threshold with an anomalously small hadronic width (few MeV). We do not find this solution physically meaningful. We searched for a local minimum in the 1340–1400 MeV mass range but none was found. Then we forced the pole position to  $(1380 - i90) \text{ MeV}$  [13]. The  $\chi^2$  improved for some data, for other data it became worse. Overall, the  $\chi^2$  improved for two-body reactions by 310 units,

and the likelihood for the fit to the CLAS data deteriorated by slightly more than 3000, but this change is hardly visible when data and fit are compared. When the data are restricted to two-body reactions and the width of the low-mass pole is fixed to 180 MeV, the mass scan shows a shallow minimum for a low-mass resonance at  $(1387 \pm 3) \text{ MeV}$ . In the two-pole solution, mass and width of  $\Lambda(1405)$  did not change significantly but the residues were altered. The residues for the hypothetical  $\Lambda(1380)$  and for  $\Lambda(1405)$  are given in Table 3. The values cover the range when the  $\Lambda(1380)$  properties are varied from 1350 to 1400 MeV and the width from 120 to 220 MeV.

### 5 Comparison with other work

Our pole positions for the  $\Lambda(1405)$  resonance in the one and two-pole solutions are in good agreement with the position of the high-mass pole of fits based on a chiral unitary coupled-channel approach. Table 4 compares our results with those obtained in Refs. [13, 14, 16]. Evidently, 1405 MeV is not the correct mass when only modern analyses are used in the comparison.

The authors of Ref. [21] have performed a comparative analysis of the different approaches based on the chiral SU(3) dynamics. The different approaches lead to rather different predictions for the  $K^-p$  and  $K^-n$  S-wave elastic scattering amplitudes. In particular the extrapolation to subthreshold energies yields a wide spectrum of results. The amplitudes are shown in Fig. 9 and compared to our  $K^-p$  S-wave elastic scattering amplitudes. Our amplitudes are well within the range of amplitudes derived in models based on the chiral SU(3) dynamics. The real part of our scattering amplitude vanishes at about 1420 MeV, the imaginary part reaches a maximum of about 2 fm. The best consistency is achieved with the elastic scattering amplitudes derived in Refs. [13], [14] (black dashed and blue dashed-dotted curves in Fig. 9). The  $K^-n \rightarrow K^-n$  scattering amplitudes scatter considerably. This amplitude can be constrained by a measurement of the energy shift and width of the 1S level of kaonic deuterium [62, 63].

Friedman and Gal have used the amplitudes shown in Figs. 9 in the construction of  $K^-$ -nucleus optical potentials that fit kaonic atom strong-interaction data across the periodic Table [64]. The optical potential was constrained by the fraction of single-nucleon absorption. Only the  $\bar{K}^- - N$  amplitudes determined in Refs. [11, 13] and the amplitudes derived here were found to be consistent with the known absorption fractions [64, 65].

The  $\pi\Sigma \rightarrow \pi\Sigma$  amplitude is, of course, not directly measurable but can be extracted from the fits. In Fig. 10, top sub-figures, it is compared to the amplitude derived in Ref. [19]. Even though the two amplitudes differ, they are in qualitative

**Table 2** Residues for  $\bar{K}N \rightarrow \Lambda(1405) \rightarrow \bar{K}N, \pi \Sigma$  and for  $\Lambda(1520) \rightarrow \bar{K}N, \pi \Sigma$  in the one-pole solution

Pole position $M, -\frac{i}{2}\Gamma$ (1421 ± 3, -i(23 ± 3)) MeV		
Residues	Magnitude	Phase
$2 \cdot \text{Res}(\bar{K}N \rightarrow \Lambda(1405) \rightarrow \bar{K}N)/\Gamma$	$3.3 \pm 0.3$	$-(28 \pm 7)^\circ$
$2 \cdot \text{Res}(\bar{K}N \rightarrow \Lambda(1405) \rightarrow \pi \Sigma)/\Gamma$	$2.1 \pm 0.1$	$-(6 \pm 3)^\circ$
Pole position $M, -\frac{i}{2}\Gamma$ (1516.9 ± 0.5, -i(7.6 ± 0.5)) MeV		
Residues:	Magnitude	Phase
$2 \cdot \text{Res}(\bar{K}N \rightarrow \Lambda(1520) \rightarrow \bar{K}N)/\Gamma$	$0.45 \pm 0.01$	$-(18 \pm 3)^\circ$
$2 \cdot \text{Res}(\bar{K}N \rightarrow \Lambda(1520) \rightarrow \pi \Sigma)/\Gamma$	$0.43 \pm 0.02$	$-(15 \pm 3)^\circ$

**Table 3** Residues for  $\bar{K}N \rightarrow \Lambda(1380) \rightarrow \bar{K}N, \pi \Sigma$  and for  $\Lambda(1405) \rightarrow \bar{K}N, \pi \Sigma$  in the two-pole solution. The lower-mass pole is fixed to (1380 - i90) MeV

Pole position $M, -\frac{i}{2}\Gamma$ : (1380 - i90) MeV		
Residues	Magnitude	Phase
$2 \cdot \text{Res}(\bar{K}N \rightarrow \Lambda(1380) \rightarrow \bar{K}N)/\Gamma$	$2.20 \pm 0.15$	$-(70 \pm 10)^\circ$
$2 \cdot \text{Res}(\pi \Sigma \rightarrow \Lambda(1380) \rightarrow \pi \Sigma)/\Gamma$	$0.95 \pm 0.25$	$-(157 \pm 9)^\circ$
Pole position $M, -\frac{i}{2}\Gamma$ : (1423 ± 3, -i(20 ± 3)) MeV		
Residues	Magnitude	Phase
$2 \cdot \text{Res}(\bar{K}N \rightarrow \Lambda(1405) \rightarrow \bar{K}N)/\Gamma$	$2.3 \pm 0.3$	$-(17 \pm 11)^\circ$
$2 \cdot \text{Res}(\bar{K}N \rightarrow \Lambda(1405) \rightarrow \pi \Sigma)/\Gamma$	$2.15 \pm 0.20$	$-(108 \pm 12)^\circ$

**Table 4** Comparison of the pole position of  $\Lambda(1405)$  with the high-mass (narrow) pole from fits based on a chiral Lagrangian

	Real part	Imaginary part	2nd pole?
This work	1421 ± 3	23 ± 3 MeV	No
[13]	1424 <sup>+7</sup> <sub>-23</sub>	26 <sup>+3</sup> <sub>-14</sub> MeV	Yes
[14], sol. 1	1417 <sup>+4</sup> <sub>-4</sub>	24 <sup>+7</sup> <sub>-4</sub> MeV	Yes
[14], sol. 2	1421 <sup>+3</sup> <sub>-2</sub>	19 <sup>+8</sup> <sub>-5</sub> MeV	Yes
[16], sol. 2	1434 <sup>+2</sup> <sub>-2</sub>	10 <sup>+2</sup> <sub>-1</sub> MeV	Yes
[16], sol. 4	1429 <sup>+8</sup> <sub>-7</sub>	12 <sup>+2</sup> <sub>-3</sub> MeV	Yes
[20]	1420 <sup>+15</sup> <sub>-21</sub>	27 <sup>+18</sup> <sub>-21</sub> MeV	Yes
[35]	1425	21 MeV	No

agreement. A completely different picture is obtained for the  $K^- p \rightarrow \Sigma \pi$  transition amplitude (see Fig. 10, bottom sub-figures). While the imaginary part of the transition amplitude at the resonance is negative in the fit of Ref. [19], it is positive in our fit. This has an important bearing for the SU(3) structure of the  $\Lambda(1405)$  resonance.

In our one-pole solution, the signs of the  $\bar{K}N \rightarrow \Lambda(1405) \rightarrow \pi \Sigma$  and  $\bar{K}N \rightarrow \Lambda(1520) \rightarrow \pi \Sigma$   $D$ -matrix coupling constants are identical. This is an important finding: The two particles,  $\Lambda(1405)$  and  $\Lambda(1520)$ , seem to have the same SU(3) structure. Under the assumption that  $\Lambda(1520)$  is an SU(3) singlet,  $\Lambda(1405)$  is a singlet, too. The determination

of the sign required the inclusion of the  $K^- p \rightarrow \pi \Sigma$  data in a mass region covering the  $\Lambda(1520)$  [47]. When these data were not included, identical fits were obtained for both relative signs. In analyses based on Effective Field Theories [10–20],  $\Lambda(1405)$  is described as mainly an SU(3) octet state.

Surprisingly, the  $\bar{K}N \rightarrow \Lambda(1405) \rightarrow \pi \Sigma$  transition amplitude changed the sign when a second pole was admitted in our two-pole solution and is now well compatible with the one found in Ref. [19]. Thus, the dominant SU(3) structure of  $\Lambda(1405)$  changes from singlet to octet when a second low-mass isoscalar resonance is enforced in the fit.

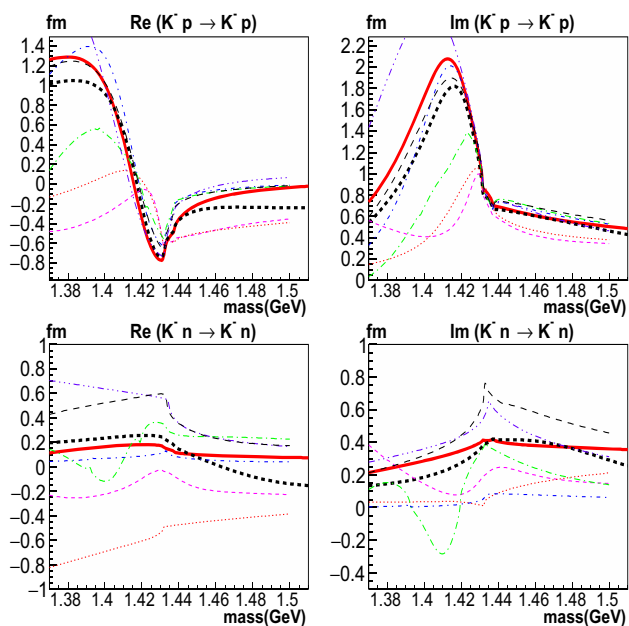


**Fig. 9**  $K^-p$  and  $K^-n$   $S$ -wave elastic scattering amplitude. The thick black curves corresponds to our one-pole  $\Lambda$  solution, the long-dash-triple-dotted curve is from [11], the black dashed curve from [13], the green and the blue dashed-dotted curves from [14], the purple dashed and the red dotted curves from [16]. See [21] for a model comparison

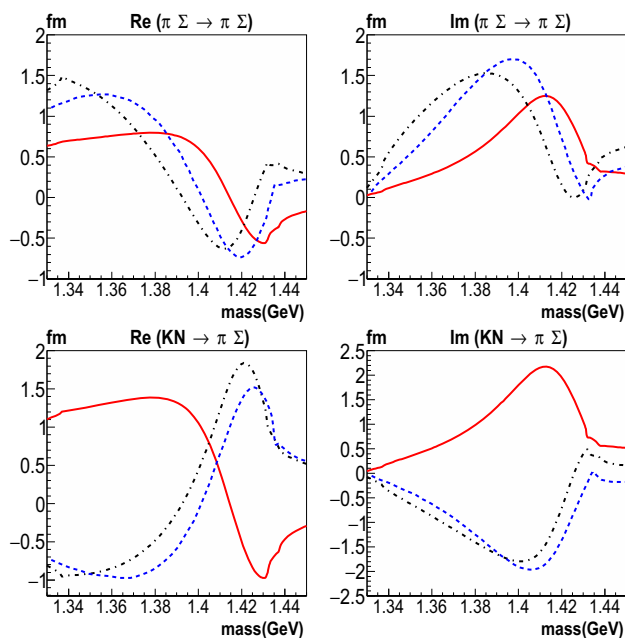


**Fig. 10** The  $\pi\Sigma \rightarrow \pi\Sigma$  and  $\bar{K}N \rightarrow \pi\Sigma$  isoscalar  $S$ -wave transition amplitudes. The solid curve represents our one-pole, the dashed-dotted curve our two-pole solution, the dashed curve is taken from Fig. 5 in Ref. [19]

## 6 Discussion and summary

We have performed a partial wave analysis of low-energy data on  $K^-p$  and  $\Sigma\pi$   $S$ -wave interactions. Analyses based on unitarized chiral perturbation theory [7–18] find two  $\Lambda^*$  resonances with  $J^P = 1/2^-$  in the region below 1500 MeV. Within our approach—that neglects constraints from the symmetry-breaking pattern of low-energy QCD—we have found two solutions that both describe reasonably well the full data set on low-energy  $K^-p$  induced interactions and the CLAS data on the low-mass range of the three  $\pi\Sigma$  charge states produced in the reactions  $\gamma p \rightarrow K^+(\pi\Sigma)$ . One solution is fully compatible with a fit with one single resonance,  $\Lambda(1405)$ , and background terms. The background consists of two or three poles below the  $\Sigma\pi$  threshold: two  $\Sigma$  poles and either no or one single  $\Lambda$  pole. The pole of the  $\Lambda(1405)$  is found at  $M_{\text{pole}} = (1421 \pm 3, -i(23 \pm 3))$  MeV. The data on  $K^-p \rightarrow \Sigma\pi$  suggest that the SU(3) structure of  $\Lambda(1405)$  is a mainly SU(3)-singlet resonance. This solution is fully compatible with quark-model predictions. Obviously, the data on  $K^-p \rightarrow \pi\Sigma$  are important for the interpretation of the  $\Lambda(1405)$  resonance. So far, the data are included only in our analysis.

We also found a second solution that offers two isoscalar poles to the fit. When mass and width are left free, unphysical solutions evolve. But by imposing mass and width of the low-mass pole to be consistent with those from Refs. [12, 13], a solution is obtained that still describes the data reasonably well. If the width is fixed, the scan for the mass provides a minimum provided the data are restricted to the two-body reactions. In this case, even the SU(3) structure is compatible with the findings from Refs. [12, 13]. We note that the fit requires large imaginary parts for the transition amplitudes.

In the two-pole solution, there exists one resonance more than the quark model predicts. The natural candidate for an additional resonance would be a  $\Lambda(1380)$ . However, there is the difficulty that in the two-pole fit, the well-established  $\Lambda(1405)$  becomes a mainly octet SU(3) state while the quark model predicts a SU(3) singlet state. We may need to consider  $\Lambda(1405)$  to be the intruder, the state that does not match to any quark model state. Alternatively, the  $\Lambda(1380)$  is the intruder; due to its large width, it overlaps with the  $\Lambda(1405)$  and could change its SU(3) structure to become an SU(3) octet state.

At present, it is difficult to judge which solution is right. Technically, the one-pole solution is from a fit where all parameters are the consequence of a free fit. This is the reason why we consider this as our preferred fit. However, we cannot rule out the possibility that constraints from chiral unitarity might lead to a convergent result for a lower-mass resonance as well.

**Acknowledgements** Open Access funding provided by Projekt DEAL. W. Weise suggested to search intensively for solutions with a second

pole. He was right, and we are grateful for his advice. We would like to acknowledge useful discussions with A. Gal and U.-G. Meißner and valuable comments from J. Révai and E. Oset. This work was supported by the Deutsche Forschungsgemeinschaft (SFB/ TR110), the Russian Science Foundation (RSF 16-12-10267), the United States Department of Energy under contract DE-AC05-06OR23177 (Jefferson Lab) and DE-FG02-87ER 40315 (Carnegie Mellon University).

**Data Availability Statement** This manuscript has no associated data or the data will not be deposited. [Authors' comment: All data used in this article are published in papers cited in the text].

**Open Access** This article is licensed under a Creative Commons Attribution 4.0 International License, which permits use, sharing, adaptation, distribution and reproduction in any medium or format, as long as you give appropriate credit to the original author(s) and the source, provide a link to the Creative Commons licence, and indicate if changes were made. The images or other third party material in this article are included in the article's Creative Commons licence, unless indicated otherwise in a credit line to the material. If material is not included in the article's Creative Commons licence and your intended use is not permitted by statutory regulation or exceeds the permitted use, you will need to obtain permission directly from the copyright holder. To view a copy of this licence, visit <http://creativecommons.org/licenses/by/4.0/>.

## References

- M.H. Alston et al., Phys. Rev. Lett. **6**, 698 (1961)
- R.H. Dalitz, S.F. Tuan, Ann. Phys. **10**, 307 (1960)
- R.H. Dalitz, T.C. Wong, G. Rajasekaran, Phys. Rev. **153**, 1617 (1967)
- R.D. Tripp, R.O. Bangerter, A. Barbaro-Galtieri, T.S. Mast, Phys. Rev. Lett. **21**, 1721 (1968)
- N. Isgur, G. Karl, Phys. Rev. D **18**, 4187 (1978)
- N. Kaiser, T. Waas, W. Weise, Nucl. Phys. A **612**, 297 (1997)
- J.A. Oller, U.-G. Meißner, Phys. Lett. B **500**, 263 (2001)
- D. Jido, J.A. Oller, E. Oset, A. Ramos, U.-G. Meißner, Nucl. Phys. A **725**, 181 (2003)
- E. Oset, A. Ramos, C. Bennhold, Phys. Lett. B **527**, 99 (2002) Erratum: [Phys. Lett. B **530**, 260 (2002)]
- A. Cieplý, J. Smejkal, Eur. Phys. J. A **43**, 191 (2010)
- A. Cieplý, J. Smejkal, Nucl. Phys. A **881**, 115 (2012)
- Y. Ikeda, T. Hyodo, W. Weise, Phys. Lett. B **706**, 63 (2011)
- Y. Ikeda, T. Hyodo, W. Weise, Nucl. Phys. A **881**, 98 (2012)
- Z.H. Guo, J.A. Oller, Phys. Rev. C **87**(3), 035202 (2013)
- M. Mai, U.-G. Meißner, Nucl. Phys. A **900**, 51 (2013)
- M. Mai, U.-G. Meißner, Eur. Phys. J. A **51**, 30 (2015)
- L. Roca, E. Oset, Phys. Rev. C **87**, 055201 (2013)
- L. Roca, E. Oset, Phys. Rev. C **88**, 055206 (2013)
- K. Miyahara, T. Hyodo, W. Weise, Phys. Rev. C **98**, 025201 (2018)
- A. Feijoo, V. Magas, A. Ramos, Phys. Rev. C **99**(3), 035211 (2019)
- A. Cieplý, M. Mai, U.-G. Meißner, J. Smejkal, Nucl. Phys. A **954**, 17 (2016)
- S. Capstick, N. Isgur, Phys. Rev. D **34**, 2809 (1986) [AIP Conf. Proc. **132**, 267 (1985)]
- L.Y. Glozman, D.O. Riska, Phys. Rept. **268**, 263 (1996)
- U. Löring, B.C. Metsch, H.R. Petry, Eur. Phys. J. A **10**, 447 (2001)
- M.M. Giannini, E. Santopinto, Chin. J. Phys. **53**, 020301 (2015)
- C. Fernandez-Ramirez, I.V. Danilkin, V. Mathieu, A.P. Szczepaniak, Phys. Rev. D **93**(7), 074015 (2016)
- G. Agakishiev et al., HADES Collaboration. Phys. Rev. C **87**, 025201 (2013)
- M. Hassanvand, S.Z. Kalantari, Y. Akaishi, T. Yamazaki, Phys. Rev. C **87**, 055202 (2013)
- K. Moriya et al., CLAS Collaboration. Phys. Rev. C **87**, 035206 (2013)
- K. Moriya et al., CLAS Collaboration. Phys. Rev. Lett. **112**, 082004 (2014)
- M. Hassanvand, Y. Akaishi, T. Yamazaki, "Clear indication of a strong  $I = 0 \bar{K}N$  attraction in the  $\Lambda(1405)$  region from the CLAS photo-production data," arXiv:1704.08571 [nucl-th]
- F.Y. Dong, B.X. Sun, J.L. Pang, Chin. Phys. C **41**, 074108 (2017)
- P.C. Bruns, M. Mai, U.-G. Meißner, Phys. Lett. B **697**, 254 (2011)
- J. Révai, Few Body Syst. **59**(4), 49 (2018)
- J. Révai, arXiv:1811.09039 [nucl-th]
- P. C. Bruns, A. Cieplý, arXiv:1911.09593 [nucl-th]
- K. S. Myint, Y. Akaishi, M. Hassanvand, T. Yamazaki, PTEP **2018**, 073D01 (2018)
- M. Niiyama et al., Phys. Rev. C **78**, 035202 (2008)
- H.Y. Lu et al., CLAS Collaboration. Phys. Rev. C **88**, 045202 (2013)
- M. Matveev, A.V. Sarantsev, V.A. Nikonov, A.V. Anisovich, U. Thoma, E. Klempt, Eur. Phys. J. A **55**, 179 (2019)
- A.V. Sarantsev, M. Matveev, V.A. Nikonov, A.V. Anisovich, U. Thoma, E. Klempt, Eur. Phys. J. A **55**, 180 (2019)
- E. Klempt, V. Burkert, L. Tiator, U. Thoma, R. Workman, "A and  $\Sigma$  excitations in the Quark Model", in preparation
- A.V. Anisovich, A.V. Sarantsev, V.A. Nikonov, V. Burkert, R.A. Schumacher, U. Thoma, E. Klempt, Hyperon IV: "Hyperon resonances from photoproduction", in preparation
- S. Prakhov et al., Crystall Ball Collaboration. Phys. Rev. C **70**, 034605 (2004)
- R.J. Hemingway, Nucl. Phys. B **253**, 742 (1985)
- T.S. Mast, M. Alston-Garnjost, R.O. Bangerter, A.S. Barbaro-Galtieri, F.T. Solmitz, R.D. Tripp, Phys. Rev. D **14**, 13 (1976)
- R. Armenteros et al., Nucl. Phys. B **21**, 15 (1970)
- W.E. Humphrey, R.R. Ross, Phys. Rev. **127**, 1305 (1962)
- M.B. Watson, M. Ferro-Luzzi, R.D. Tripp, Phys. Rev. **131**, 2248 (1963)
- M. Sakitt, T.B. Day, R.G. Glasser, N. Seeman, J.H. Friedman, W.E. Humphrey, R.R. Ross, Phys. Rev. **139**, B719 (1965)
- J. Ciborowski et al., J. Phys. G **8**, 13 (1982)
- D.N. Tovee et al., Nucl. Phys. B **33**, 493 (1971)
- R.J. Nowak et al., Nucl. Phys. B **139**, 61 (1978)
- M. Bazzi et al., SIDDHARTA Collaboration. Phys. Lett. B **704**, 113 (2011)
- M. Bazzi et al., Nucl. Phys. A **881**, 88 (2012)
- G. Colangelo, J. Gasser, H. Leutwyler, Nucl. Phys. B **603**, 125 (2001)
- I. Caprini, G. Colangelo, H. Leutwyler, Phys. Rev. Lett. **96**, 132001 (2006)
- M. Tanabashi, et al.: [Particle Data Group], Phys. Rev. D **98**, no. 3, 030001 (2018)
- E. Salpeter, H.A. Bethe, Phys. Rev. **84**, 1232 (1951)
- V.K. Magas, E. Oset, A. Ramos, Phys. Rev. Lett. **95**, 052301 (2005)
- U.-G. Meißner, U. Raha, A. Rusetsky, Eur. Phys. J. C **35**, 349 (2004)
- J. Révai, Phys. Rev. C **94**(5), 054001 (2016)
- T. Hoshino, S. Ohnishi, W. Horiuchi, T. Hyodo, W. Weise, Phys. Rev. C **96**(4), 045204 (2017)
- E. Friedman, A. Gal, Nucl. Phys. A **959**, 66 (2017)
- E. Friedman, A. Gal, private communication, (2019), Dec. 25